

# Molecular BioSystems

Accepted Manuscript



This is an *Accepted Manuscript*, which has been through the Royal Society of Chemistry peer review process and has been accepted for publication.

*Accepted Manuscripts* are published online shortly after acceptance, before technical editing, formatting and proof reading. Using this free service, authors can make their results available to the community, in citable form, before we publish the edited article. We will replace this *Accepted Manuscript* with the edited and formatted *Advance Article* as soon as it is available.

You can find more information about *Accepted Manuscripts* in the [Information for Authors](#).

Please note that technical editing may introduce minor changes to the text and/or graphics, which may alter content. The journal's standard [Terms & Conditions](#) and the [Ethical guidelines](#) still apply. In no event shall the Royal Society of Chemistry be held responsible for any errors or omissions in this *Accepted Manuscript* or any consequences arising from the use of any information it contains.



[www.rsc.org/molecularbiosystems](http://www.rsc.org/molecularbiosystems)

**Dynamic equilibrium of endogenous selenium nanoparticles in selenite-exposed cancer cells: a deep insight of the interaction between endogenous SeNPs and proteins**

Peng Bao<sup>1,2,\*</sup>, Song-Can Chen<sup>3</sup>, Ke-Qing Xiao<sup>3</sup>

<sup>1</sup> Institute of Urban Environment, Chinese Academy of Sciences, Xiamen 361021, China

<sup>2</sup> Ningbo Urban Environment Observation and Research Station, Chinese Academy of Sciences, Ningbo 315800, China

<sup>3</sup> State Key Lab of Urban and Regional Ecology, Research Center for Eco-Environmental Sciences, Chinese Academy of Sciences, Beijing 100085, P. R. China

Author for correspondence: Dr. Peng Bao,

Institute of Urban Environment, Chinese Academy of Sciences, Xiamen 361021, China

a. Tel: +86-574-86085998; Fax: +86-574-86784810; E-mail: [pbao@iue.ac.cn](mailto:pbao@iue.ac.cn).

**Abstract**

Elemental selenium (Se) was recently found to exist as endogenous nanoparticles (i.e., SeNPs) in selenite-exposed cancer cells. By sequestering critical intracellular proteins, SeNPs appear capable of giving rise to multiple cytotoxicity mechanisms including inhibition of glycolysis, glycolysis-dependent mitochondrial dysfunction, microtubule depolymerization and inhibition of autophagy. In this work, we reveal a dynamic equilibrium of endogenous SeNPs assembly and disassembly in selenite-exposed H157 cells. Endogenous SeNPs are observed both in the cytoplasm and in organelles. There is an increase in endogenous SeNPs between 24 h and 36 h, and decrease between 36 h and 72 h according to transmission electron microscopy results and UV-Vis measurements. These observations imply that elemental Se in SeNPs could be oxidized back into selenite by scavenging superoxide radicals and ultimately re-reduced into selenide; then the assembly and disassembly of SeNPs proceeds simultaneously with the sequestration and release of SeNPs high-affinity proteins. There is also a possibility that reduction of elemental Se to selenide pathway may lie in selenite-exposed cancer cells which results in assembly and disassembly of endogenous SeNPs. Genome-wide expression analysis results shows that endogenous SeNPs significantly altered the expression of 504 genes, compared to control. The endogenous SeNPs induced mitochondrial impairment and decreasing of annexin A2 level can lead to inhibition of cancer cells invasion and migration. This dynamic flux of endogenous SeNPs amplifies their cytotoxic potential in cancer cells, thus provide a starting point to design more efficient intracellular self-assembling

systems for overcoming multidrug resistance.

### 1. Introduction

Selenium (Se) is a micronutrient that has potential applications in chemoprevention. This biological activity of Se is dependent on its speciation. Selenite, the most commonly-used Se compound, exhibits efficient inhibition of the proliferation of malignant cells; there is an inverse relationship between resistance to chemotherapy and sensitivity to selenite.<sup>1,2</sup> The multiple mechanisms of selenite-induced cytotoxicity in cancer cells are thought to arise from its metabolites.

Selenite is readily reduced by glutathione (GSH) to selenodiglutathione (GSSeSG), which further reduces to selenopersulfide (GSSeH) and elemental Se.<sup>3,4</sup> Glutathione reductase also reduces GSSeSG to hydrogen selenide (HSe<sup>-</sup>) in the presence of NADPH.<sup>5</sup> Generation of elemental Se presumably occurs during the reaction of HSe<sup>-</sup> and oxygen, which can result in oxidative stress in cells.<sup>6</sup> As a substrate of both glutaredoxin and thioredoxin and their respective oxidoreductase systems, GSSeSG is slightly more toxic than selenite.<sup>7,8</sup> HSe<sup>-</sup> is possibly toxic to cells by perturbing intracellular redox balance due to consumption of intracellular GSH.<sup>9</sup>

Elemental Se is generally considered nontoxic due to its insolubility. We have recently shown, for the first time, that intracellular metabolism of selenite generates endogenous Se nanoparticles (SeNPs) in cancer cells.<sup>10</sup> Critical proteins bind with high-affinity to elemental Se during SeNPs self-assembly; these include glycolytic enzymes, insoluble tubulin and heat shock proteins 90 (HSP90). Sequestration of glycolytic enzymes by SeNPs dramatically inhibits ATP generation, which leads to the inhibition of glycolysis and glycolysis-dependent mitochondrial dysfunction.

Sequestration of insoluble tubulin leads to microtubule depolymerization, altering microtubule dynamics. HSP90 sequestration leads to degradation of its downstream effectors *via* autophagy, ultimately resulting in a cell-signaling switch to apoptosis. Additionally, the surface effects of SeNPs generated oxidative stress, contributing even more to selenite-induced cytotoxicity.<sup>10</sup>

Mitochondria play a central role when responding to selenite toxicity. Cox is a critical enzyme in the mitochondrial electron transport chain and reduced Cox level may affect mitochondrial structure. Glucose depletion decreases levels of mitochondrial proteins, including respiratory complex I and complex III in hepatoma cells.<sup>11</sup> Inhibition of mitochondrial complex I by metformin results in inhibition of cancer-cell proliferation, and even induction of cell death upon glucose deprivation.<sup>12</sup> We then proposed to evaluate the level of Cox I, Cox II and Cox IV in non-small lung cancer cell line H157 under the exposure of selenite. Recent studies have identified a calcium-dependent phospholipid-binding protein annexin A2 (ANXA2), as an important mediator of malignant transformation and development of hepatocellular carcinoma.<sup>13,14</sup> In this regard, we also tried to figure out the interaction of endogenous SeNPs and annexin A2, and the subsequent inhibition of H157 cells invasion and metastasis.

When the dynamics of elemental Se were examined in lung cancer A549 cells by extended X-ray absorption fine structure (EXAFS), it was found that the levels of intracellular elemental Se increased between 4 and 72 h, and decreased slightly between 48 and 72 h.<sup>15</sup> As we have revealed that elemental Se in cancer cells

presented as SeNPs,<sup>10</sup> we therefore propose that there is a dynamic process of endogenous SeNPs formation in cells. In this study, we report the dynamic equilibrium of endogenous SeNPs assembly and disassembly in non-small lung cancer H157 cells. This dynamic flux of endogenous SeNPs will undoubtedly amplify their toxicity in cancer cells, because of the increased difficulty to mediate a dynamic response to resist different toxic pathways. These results not only highlight the importance of endogenous SeNPs cytotoxicity towards chemoprevention, but also in the event of excessive intake of Se.

## **2. Materials and methods**

### **2.1 Cell culture**

H157 cells were grown in RPMI medium with 10% FBS and 1% PEST at 37°C in a 5% CO<sub>2</sub> incubator. A549 or human gastric carcinoma MGC-803 cells were grown in DMEM medium with 10% FBS, 1% PEST and 2% glutamine at 37°C in a 5% CO<sub>2</sub> incubator. All experiments were adjusted for consistency. After pre-incubation, the culture was treated with sodium selenite (10 µM) for 24 h.

### **2.2 Viability measurements**

Viability was measured by means of the MTT (3-[4, 5-dimethylthiazol-2-yl]-2, 5-diphenyltetrazolium bromide) assay in 96-well cell culture plates (Nunc) modified according to Olm et al (2009).<sup>16</sup> Cells were counted in a Burke's chamber, and 10,000 cells per well (200,000 cells/mL) were plated and pre-incubated for 24 h to allow adhesion. After pre-incubation, the medium was discarded, and treated with a series of concentrations of sodium selenite (0.25, 0.5, 1.0, 5.0, 10, or 20 µmol/L in 50 µL

medium) for 24 h in five replicates. After 24 h, 15  $\mu\text{L}$  (per 80  $\mu\text{L}$  cell culture) of Cell Quanti-MTT<sup>TM</sup> reagent (Quanti-MTT<sup>TM</sup> cell viability assay kits, BioAssay systems, USA) was added to each well, and incubated for 4 h at 37°C. Solubilization solution (100  $\mu\text{L}$ ) was added, and the mixture mixed gently on an orbital shaker for 1 h at room temperature. Plates were read at 570 nm (SpectraMax 190, Molecular Devices, USA). Medium and reagent backgrounds were subtracted, and each data point was plotted relative to control cells.

### **2.3 Identification of the distribution of endogenous SeNPs in H157 cells, and characterization of SeNPs**

The cell pellets (0, 24, 36 and 72 h selenite exposure and without selenite treatment) were first washed with PBS and then fixed *in situ* overnight at 4°C with 4% glutaraldehyde buffered with 0.1 M phosphate, pH 7.4. Cell pellets were then fixed in 1% osmium tetroxide buffered with veronal for 1h. Then they were dehydrated in an alcohol series (10 min each in 25%, 50%, 75%, 85%, 95%, and in 100% ethanol twice); then, cell pellets were embedded in Epon 812 for ultrathin sections. Identification of endogenous SeNPs was performed by transmission electron microscopy (TEM; Hitachi H-7500). Extraction of SeNPs from cells was provided in section 2.8.

### **2.4 RNA extraction, sequencing and assembly of nuclear genome**

H157 cell cultures after 24 hr +/- sodium selenite (10  $\mu\text{M}$ ) were pelleted and mRNA was extracted using TruSeq RNA Sample Prep Kit following the manufacturer's guidance. Aliquots of mRNA were then pooled for conversion into

cDNA and sequenced to obtain transcriptomic data. The quality of cDNA used for sequencing was assessed by the PicoGreen assay (Quant-iT PicoGreen dsDNA Assay Kit, Invitrogen, P7589) and an Agilent Bioanalyzer (Agilent 2100 Bioanalyzer, Agilent, 2100; Agilent High Sensitivity DNA Kit, Agilent, 5067-4626); in all cases, this satisfied all quality-control metrics. The most accurate possible gene models (RNA-seq methods) were used to generate an assembled transcriptome and to map transcriptome reads to the genome; we adopted Illumina sequencing on pooled samples of cDNA that had been made from polyA-selected RNA. This cDNA was sequenced using the Illumina short insert paired-end sequencing (SIPES) protocol, and pairs the sequencing reads at ~200 bp separation. Sequencing reads were trimmed, except that all reads as long as 50 bp were retained. A total of 53,498,910 and 51,796,643 raw reads for selenite-treated and untreated H157 cells, respectively were determined, and then 43,263,814 and 41,732,190 reads for selenite-treated and untreated H157 cells, respectively survived the trimming, with a mean trimmed read length of 50.7 nts.

Assembly was performed and followed by measuring and comparing their quality. We obtained 155-bp mate-paired reads from DNA fragments of average length of 250-bp (standard deviation for the distribution of inner distances between mate pairs is approximately 50 bp). Trimmed adaptor sequences, and sequence quality lower than Q20 (sliding window size 5 bp), led us to abort sequences that were lower than 50 bp. Optimized RNA-Seq reads (most of quality distributed between 35 to 40) were separately aligned to the human genome (GRCh37.73) using TopHat software

(version 2.0). Annotated transcripts were obtained from the Ensembl database.

## **2.5 Quantitative real-time polymerase chain reaction of Cox-1, Cox-2, Cox-4 gene**

The cDNAs of Cox-1, Cox-2, Cox-4 and 18S RNA were amplified using the primer pairs shown in table S1. SYBR FAST qPCR Kit (Master Mix (2×) Universal, KAPA Biosystems, USA) was used for quantitative reverse-transcriptase polymerase chain reaction (qRT-PCR) reactions, and performed on an ABI Prism 7900 sequence detection system (Applied Biosystems, Foster City, CA) as described previously.<sup>17</sup> The relative abundance of a transcript was represented by the threshold cycle of amplification ( $C_T$ ). The comparative  $C_T$  method was calculated according to the manufacturer's instructions. The expression level of Cox-1 relative to the baseline level was calculated as  $2^{-\Delta C_T(\text{Cox-1})}$ , where  $\Delta C_T$  is (average Cox-1  $C_T$  - average 18s  $C_T$ ) and is  $C_T$  (average  $C_T$ -treated sample - average  $C_T$ -untreated sample).

## **2.6 Cox-1, Cox-2, Cox-4 and ANXA2 immunoblotting assays**

Total cell lysates were prepared as previously described.<sup>17</sup> Cells were washed twice with pH 7.4 phosphate buffered saline and suspended in lysis buffer (1.5% n-dodecyl  $\beta$ -maltoside (Sigma Aldrich, St. Louis, MO)), which containing protease inhibitor tablets (Complete tablets; Roche, IN). Protein concentrations were measured by the DC Protein assay (Bio Rad, Hercules, CA). Equal amounts of protein were subjected to (SDS)-polyacrylamide gels followed by transfer to nitrocellulose membranes. Membranes were probed with anti-Cox-1 1:1000, anti-Cox-2 1:500, anti-Cox-4 1:2000, anti-human ANXA2 1:500 (Santa Cruz Biotechnology Inc),

anti- $\alpha$ -tubulin 1:2000 (Sigma Aldrich, St. Louis, MO), Detection was performed by the enhanced chemical luminescence method (Pierce, Rockford, IL).<sup>18</sup>

### **2.7 Wound healing assay**

Cells were plated ( $1 \times 10^4$  per chamber) in an 8-well chamber slide. The cells were incubated for 24 hours to allow formation of a monolayer. A wound was created in the monolayer with a 1000  $\mu$ l pipette tip. Cells were washed once with RPMI to remove any detached cells and pictures were taken of the wounds at 0 hour time point. Serum-free DMEM, untreated medium and selenite-treated media was added to the wounded cells. The cells were incubated at 37°C under 5.0% CO<sub>2</sub>. Images were taken to determine the amount of cell movement from the wound edge at 24 hours time point by using a phase contrast inverted microscope (Nikon Eclipse Ti) equipped with a digital camera. Wound closure was quantified by measuring the area of the wound using ipwin32 software.

### **2.8 Extraction and UV-Vis spectroscopy of SeNPs**

Cell culture suspensions treated with selenite (10  $\mu$ M) for 24 h were first ultrasonicated (SCIENTZ, JY92-2D) for 60 s at 200 W, and then centrifuged at 11,000 rpm/min (centrifuge, eppendorf 5804R) in order to collect suspended SeNPs. Adherent cells were digested with pancreatic enzymes and then ultrasonication for 60 s at 200 W after collection post-centrifuge. The ruptured cell mixture was centrifuged at 2000 rpm/min to remove cellular debris, and the suspension further centrifuged at 11,000 rpm/min to collect SeNPs. These two components for SeNPs were combined for UV-Vis measurements. UV-Vis measurements were acquired on a microplate

reader (SpectraMax 190, Molecular Devices, USA). The SeNPs collected from H157 cells and SeNPs standards were suspended in 1.0 ml double-distilled water. UV-Vis spectrophotometry was performed using 96-well plates. The wave length scanning was performed from 230 to 500 nm at 1.0 nm wavelength resolution, and SeNPs was monitored at around 275 nm.<sup>19</sup> In quartz cuvettes, the standards for SeNPs were prepared in 50 mM Tris-HCl buffer (pH 7.0) supplemented with BSA, 0.5 mM selenite and 4 mM reduced glutathione.<sup>20</sup>

### 3. Results and discussion

#### 3.1 Viability and formation of endogenous SeNPs in selenite-exposed H157 cells

We initially observed that selenite inhibited growth of H157 cells after they were exposed to different concentrations of sodium selenite. Dose-dependent effects of sodium selenite on the viability of H157 cells show that selenite ( $\geq 10 \mu\text{M}$ ) significantly inhibits cell growth up to 80% (**Figure 1A**). Indirect immunofluorescence shows that microtubules exhibit an integrated structure in control cells but are dispersed following exposure to 10  $\mu\text{M}$  selenite (**Figure 1B-D**). These results agree with previous studies.<sup>10,21</sup> This growth inhibition is caused by apoptosis, demonstrated by analysis using flow cytometry.<sup>21</sup>

#### 3.2 Formation of endogenous SeNPs

The morphology and distribution of endogenous SeNPs in selenite-exposed H157 cells are shown in a stained cell monolayer (**Figure 2C-2E**), while no endogenous SeNPs generated in without selenite treatment (**Figure 2A**) and 0 hour selenite exposure (**Figure 2B**). Endogenous SeNPs are observed both in the

cytoplasm and in organelles. The amount of endogenous SeNPs at 36 h is more than in 24 h. The amount of endogenous SeNPs decreased distinctly at 72 h which less than in 24 h. TEM image of SeNPs isolated from H157 cells is shown in Figure 2F.

### 3.3 Genome-wide expression analysis of selenite-exposed H157 cells

Selenite exposure significantly ( $P < 0.05$ ) altered the expression of 504 genes, compared to control (see supporting information, **Table S1**). Of these, 218 genes showed decreased expression, while 286 were elevated. Of 51,796,643 and 53,498,910 pairs of reads generated, 80.4% and 75.3% had at least one end mapped to the reference genome (**Tables S1**). Mitochondrial RNA (mtRNA) all appeared significantly down-regulated with hundreds of fold-changes, suggesting an inhibition pathway of mitochondrial function (**Table S1**). This study for the first time reveals the response of cancer cells H157 to hyperdose selenite at the transcriptome level, therefore provides in-depth information about the impact of selenite on cancer cells.

### 3.4 Decreased level of Cox-1, Cox-2, Cox-4

Subunits of complex IV are encoded by both the nuclear and mitochondrial genomes. We investigated whether the alteration in complex IV activity was due to lower levels of cytochrome c oxidase protein encoded by the mitochondrial genome. Therefore, we examined the expression of Cox I, Cox II and Cox IV mRNA by RT-PCR. The results showed that the Cox I, Cox II and Cox IV mRNA level was significantly reduced in 10  $\mu$ M selenite-exposed cells, and was less than 30, 30 and 20 % of the values for control group, respectively (**Figure 3A**), while slightly increase was observed in 0.25  $\mu$ M selenite-exposed cells (**Figure 3A**). The protein level of

Cox I, Cox II and Cox IV was significantly reduced in selenite-exposed cells (**Figure 3B**). For 0.25  $\mu\text{M}$  selenite-exposed cells, the protein level of Cox I, Cox II and Cox IV was 56, 34 and 46 %, respectively, compared to control group. For 10  $\mu\text{M}$  selenite-exposed cells, the protein level of Cox I, Cox II and Cox IV was 57, 48 and 42 %, respectively, compared to control group. The Cox IV mRNA level was not significantly reduced in 10  $\mu\text{M}$  selenite-exposed cells compared to Cox I and Cox II (**Figure 3A**). Taken together, the discoordinate expression of Cox I, Cox II and Cox IV mRNA, and Cox I, Cox II and Cox IV protein suggest post-transcriptional regulation of Cox I, Cox II and Cox IV by endogenous SeNPs.

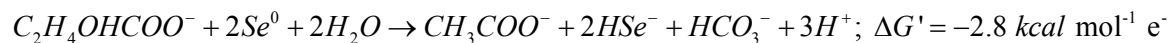
### 3.5 Decreasing level of ANXA2 inhibits proliferation of H157 cells in vitro

Selenite exposure significantly decreased annexin A2 level especially in 10  $\mu\text{M}$  selenite treatment (**Figure 4A**). To determine whether endogenous SeNPs-induced decreasing of annexin A2 level could affect H157 cells migration, the wound healing assay was performed. The effects of annexin A2 deficiency on proliferation of H157 cells are shown in Figure 5B. At 24 h, the selenite-exposed cells showed significantly lower proliferation potential than the control cells ( $P < 0.05$ ) (**Figure 4B**). Treatment of H157 cells for 24 h with selenite caused a concentration-dependent inhibition of wound closure with respect to control cells and the relative inhibitory ratio was 20% for 5  $\mu\text{M}$  selenite treatment and 30% for 10, 20, and 30  $\mu\text{M}$  selenite treatment. This result explained the previous studies that selenium administration can retard the growth of prostate cancer cells.<sup>22</sup>

### 3.6 Dynamic equilibrium of intracellular SeNPs assembly

The presence of SeNPs could be observed because of its surface plasmon resonance peak appears around 275 nm (**Figure 5**).<sup>19</sup> There was an increase in endogenous SeNPs between 24 h and 36 h, and decrease between 36 h and 72 h according to the UV-Vis measurements (**Figure 5**). These observations imply that elemental Se in SeNPs could be metabolized into other forms of Se. SeNPs have scavenging effects on free radicals, including carbon-centred free radicals ( $R\cdot$ ) generated from 2,2'-azo-bis-(2-amidinopropane) hydrochloride (AAPH), the relatively stable free radical 1,1-diphenyl-2-picrylhydrazyl (DPPH), the superoxide anion ( $O_2^{\cdot-}$ ) generated from the xanthine/xanthine oxidase (X/XO) system, and singlet oxygen ( $^1O_2$ ) generated by irradiated hemoporphyrin *in vitro*.<sup>23</sup> We deduced that endogenous SeNPs could scavenge superoxide radicals in cancer cells. On this basis, we propose a hypothetical schematic diagram demonstrating intracellular dynamic cycle of endogenous SeNPs (**Figure 6**). In this dynamic cycle, elemental Se might be re-oxidized by superoxide radicals into selenite, and finally reduced into elemental Se once again. This process may consume a portion of the superoxide radical content, but the net oxygen radical level was increased during the whole dynamic cycle of endogenous SeNPs assembly and disassembly.

On the other hand, *Bacillus selenitireducens*, a selenite-respiring bacterium, can produce significant amounts of selenide from elemental Se. Microbial reduction of elemental Se to selenide occurred in estuarine sediments was also observed.<sup>24</sup> The free energies for dissimilatory reduction of elemental Se to selenide by bacteria with the incomplete oxidation of the electron donor lactate to acetate are given as follows:



Further effort should be made to justify if there is reduction of elemental Se to selenide pathway in selenite-exposed cancer cells shown as **Figure 7**.

Additionally, more high-affinity proteins were involved in the dynamic cycle of endogenous SeNPs, and this will aggravate the impact of endogenous SeNPs cytotoxicity, such as inhibition of glycolysis, glycolysis-dependent mitochondrial dysfunction, microtubule depolymerization and inhibition of autophagy.<sup>10</sup> The amount of *in vivo* Se species has been studied in both cell and animal models.<sup>15,25,26</sup> The percentage of elemental Se detected by EXAFS increased from 37% at 4 h to 55% at 48 h, before decreasing to 49% at 72 h in lung cancer H549 cells.<sup>15</sup> This result supports our finding that endogenous SeNPs assembly is a dynamic flux process in cancer cells. Hyperdose selenium was usually recommended during cancer therapy according to experience.<sup>27,28</sup> A recent research offered the same strategy for overcoming multidrug resistance (MDR) by means of intracellular self-assembly of taxol nanoparticles in cancer cells.<sup>29</sup> This result provides the reasonable guidance of selenium using strategies on cancer therapy.

#### 4. Conclusions and remarks

The endogenous SeNPs induced mitochondrial impairment and decreasing of annexin A2 level can lead to inhibition of cancer cells invasion and migration. The results complete the understanding of endogenous SeNPs toxicity. The dynamic flux of SeNPs undoubtedly amplifies their endogenous cytotoxic impact on cancer cells,

because it is much more difficult to dynamically respond on multiple fronts. This non-specificity toxic mechanism of endogenous SeNPs might make selenium a non-resistant chemotherapeutics to cancer cells which can generate endogenous SeNPs under selenium exposure. More recently, the combination of X-ray absorption spectroscopy (XAS) and X-ray fluorescence microscopy (XFM) offers an alternative for determining the speciation and distribution of Se *in vivo* and provides information about elemental Se distributions retained in intact samples, hints the possibility of metabolic generation of endogenous SeNPs in tumor tissue.<sup>10,25,26</sup> In addition, this result also implies the metabolism of artificial SeNPs *in vivo*. The study will fill gap between the efficacy observed in laboratory studies and the mixed results of clinical trials, thus has significant implications for public health. This result will be a starting strategy for scientists to design more efficient intracellular self-assembling systems for treating cancer and so that overcoming multidrug resistance.

### **Acknowledgements**

This work was financially supported by the National Natural Science Foundation of China (No. 41090280) and (No. 41090284).

## References

- 1 L. Björkhem-Bergman, K. Jönsson, L. C. Eriksson, J. M. Olsson, S. Lehmann, C. Paul and M. Björnstedt, *Biochem Pharmacol*, 2002, **63**, 1875–1884.
- 2 G. Nilsson, X. Sun, C. Nyström, A.-K. Rundlöf, A. P. Fernandes, M. Björnstedt and K. Dobra, *Free Radical Biol Med*, 2006, **41**, 874–885.
- 3 J. Li, L. Zuo, T. Shen, C. M. Xu and Z. N. Zhang, *J Trace Elem Med Biol*, 2003, **17**, 19–26.
- 4 Y. Zou, P. Niu, J. Yang, J. Yuan, T. Wu and X. Chen, *Cancer Biol Ther*, 2008, **7**, 689–696.
- 5 R. R. Cavalieri, K. G. Scott and E. Sairenji, *J Nucl Med*, 1966, **7**, 197–208.
- 6 A. Tarze, M. Dauplais, I. Grigoras, M. Lazard, N. T. Ha-Duong, F. Barbier, S. Blanquet and P. Plateau, *J Biol Chem*, 2007, **282**, 8759–8767.
- 7 E. Rudolf, K. Rudolf and M. Cervinka, *Cell Biol Toxicol*, 2008, **24**, 123–141.
- 8 M. Lo, Y. Z. Wang and P. W. Gout, *J Cell Physiol*, 2008, **215**, 593–602.
- 9 O. W. Griffith, *Free Radical Biol Med*, 1999, **27**, 922–935.
- 10 P. Bao, Z. Chen, R. Z. Tai, H. M. Shen, L. M. Francis and Y. G. Zhu, *J Proteome Res*, 2015, **14**, 1127–1136.
- 11 Y. C. Hsu, H. C. Lee, Y. H. Ping, T. Y. Liu, W. Y. Lui and C. W. Chi, *Mol Cancer Res*, 2007, **5**, 923–932.
- 12 W. W. Wheaton, S. E. Weingerg, R. B. Hamanaka, S. Soberanes, L. B. Sullivan, E. Anso, A. Glasauer, E. Dufour, G. M. Mutlu, G. S. Budigner and N. S. Chandel, *eLife*, 2014, **3**, e02242.

- 13 N. A. Lokman, M. P. Ween, M. K. Oehler and C. Ricciardelli, *Cancer Microenviron*, 2011, **4**, 199–208.
- 14 P. A. Madureira, A. P. Surette, K. D. Phipps, M. A. Taboski, V. A. Miller and D. M. Waisman, *Blood*, 2011, **118**, 4789–4797.
- 15 C. M. Weekley, J. B. Aitken, S. Vogt, L. A. Finney, D. J. Paterson, M. D. De Jonge, D. L. Howard, P. K. Witting, I. F. Musgrave and H. H. Harris, *J Am Chem Soc*, 2011, **133**, 18272–18279.
- 16 E. Olm, A. P. Fernandes, C. Hebert, A. K. Rundlöf, E. H. Larsen, O. Danielsson and M. Björnstedt, *Proc. Natl. Acad. Sci.*, 2009, **106**, 11400–11405.
- 17 A. D. Schimmer, M. P. Thomas, R. Hurren, M. Gronda, M. Pellecchia, G. R. Pond, M. Konopleva, D. Gurfinkel, I. A. Mawji, E. Brown and J. C. Reed, *Cancer Res*, 2006, **66**, 2367–2375.
- 18 M. Škrtić, S. Sriskanthadevan, B. Jhas *et al*, *Cancer Cell*, 2011, **20**, 674–688.
- 19 S. X. Yu, W. T. Zhang, W. Liu, W. X. Zhu, R. C. Guo, Y. S. Wang, D. H. Zhang and J. L. Wang, *Nanotechnology*, 2015, **26**, 145703.
- 20 C. M. Debieux, E. J. Dridge, C. M. Mueller, P. Splatt, K. Paszkiewicz, I. Knight, H. Florance, J. Love, R. W. Titball, R. J. Lewis, D. J. Richardson and C. S. Butler, *Proc. Natl. Acad. Sci.*, 2011, **108**, 13480–13485.
- 21 K. Shi, Q. Jiang, Z. Li, L. Shan, F. Li, J. An, Y. Yang and C. Xu, *J Hematol Oncol*, 2013, **6**, 7.
- 22 J. D. Morris, R. Pramanik, X. Zhang, A. M. Carey, N. Ragavan, F. L. Martin and G.

- H. Muir, *Cancer Lett*, 2006, **239**, 111–22.
- 23 B. Huang, J. Zhang, J. Hou, C. Chen, *Free Rad Biol Med*, 2003, **35**, 805–813.
- 24 Y. V. Nancharaiah, P. N. L. Lens, *Microbiol Mol Biol Rev*, 2015, **29**, 1.
- 25 C. M. Weekley, A. Shanu, J. B. Aitken, S. Vogt, P. K. Witting and H. H. Harris, *Metallomics*, 2014, **6**, 1602.
- 26 C. M. Weekley, J. B. Aitken, P. K. Witting and H. H. Harris, *Metallomics*, 2014, **6**, 2193–2203.
- 27 C. M. Weekley, and H. H. Harris, *Chem. Soc. Rev*, 2013, **42**, 8870–8894.
- 28 E. Jablonska, and M. Vinceti, *J Environ Sci Health C Environ Carcinog Ecotoxicol Rev*. 2015, DOI:10.1080/10590501.2015.1055163.
- 29 Y. Yuan, L. Wang, W. Du, Z. Ding, J. Zhang, T. Han, L. N. An, H. F. Zhang and G. L. Liang, *Angew. Chem*, 2015, **127**, 9836–9840.

Legends of figures

**Figure 1.** Dose-dependent effects of sodium selenite on the viability of H157 cells (A). Apoptosis in H157 cells exhibited by indirect immunofluorescence. The cells were harvested after selenite exposure for 24 h, and microtubules were indirectly labelled with a  $\beta$ -tubulin primary antibody and FITC-conjugated secondary antibody (green). Nuclear stained with DAPI (blue). Control (C); selenite (10  $\mu$ M) (B, D). This experiment was repeated three times. Scale bar = 10  $\mu$ m.

**Figure 2.** TEM photomicrographs of endogenous SeNPs formation in H157 cells (green cycle). (A) without selenite treatment; (B) 0 h selenite exposure; (C) 24 h selenite exposure; (D) 36 h selenite exposure; (E) 72 h selenite exposure. Blue arrows point to endogenous SeNPs on image. (F) TEM image of SeNPs extracted from H157 cells.

**Figure 3.** Relative transcript abundance of Cox-1, Cox-2 and Cox-4 in H157 cells (A). Western blotting images of Cox-1, Cox-2 and Cox-4 level in H157 cells (B).

**Figure 4.** Suppressive effect of endogenous SeNPs mediated annexin A2 decreasing on the invasion and migration potential of H157 cells. A: Representative Western blotting images of annexin A2 level in H157 cells; B: Wound healing in DMEM cultures after 24h incubation with 0–20 mM of selenite.

**Figure 5.** Dynamics of SeNPs in cell line H157 at the time point of 0 h, 24 h, 36 h and 72 h ( $n=3$ ). Treatment without selenite is shown as green line. The region of SeNPs absorption is indicated by blue column (around 275 nm).

**Figure 6.** Putative pathway one: dynamic equilibrium of SeNPs metabolism in cancer

cells.  Selenide ions;  Elemental selenium;  Selenite;  Proteins sequestered by SeNPs;  Newly involved proteins.

**Figure 7.** Putative pathway two: dynamic equilibrium of SeNPs metabolism in cancer

cells.  Selenide ions;  Elemental selenium;  Proteins sequestered by SeNPs;  Newly involved proteins.

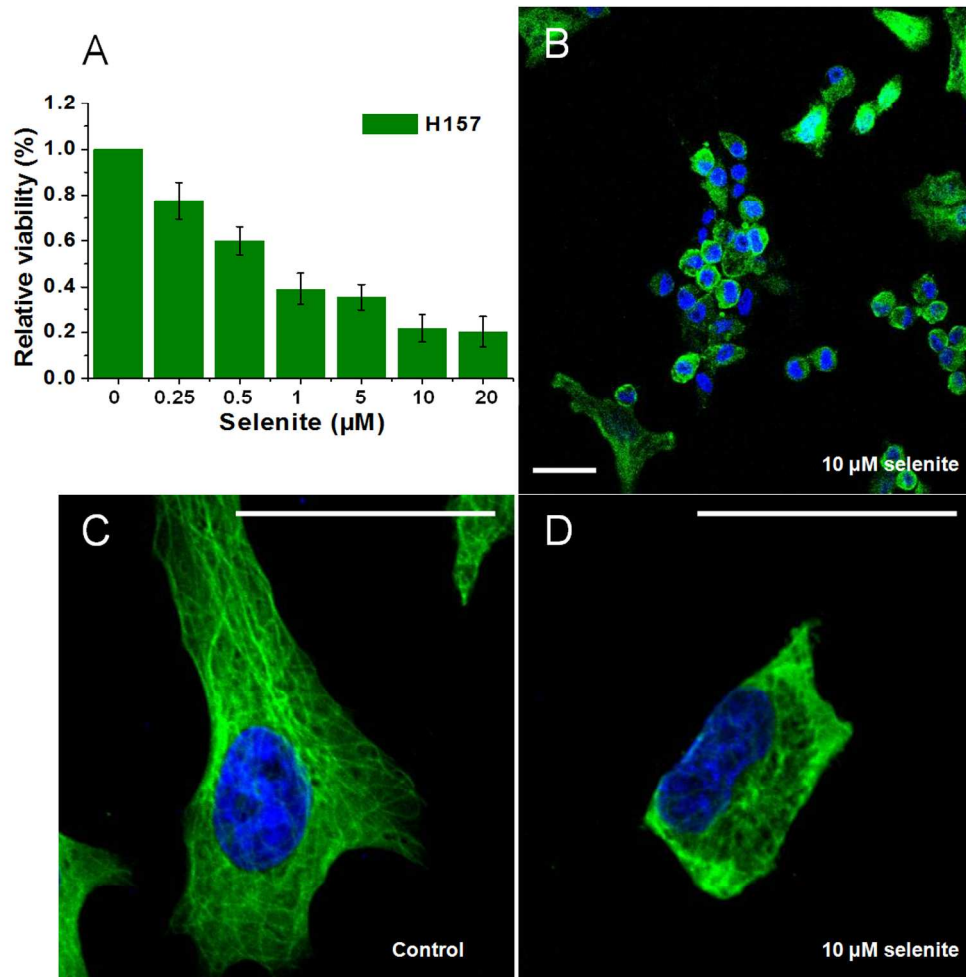


Figure 1. Dose-dependent effects of sodium selenite on the viability of H157 cells (A). Apoptosis in H157 cells exhibited by indirect immunofluorescence. The cells were harvested after selenite exposure for 24 h, and microtubules were indirectly labelled with a  $\beta$ -tubulin primary antibody and FITC-conjugated secondary antibody (green). Nuclear stained with DAPI (blue). Control (C); selenite (10  $\mu$ M) (B, D). This experiment was repeated three times. Scale bar = 10  $\mu$ m.  
418x408mm (200 x 200 DPI)

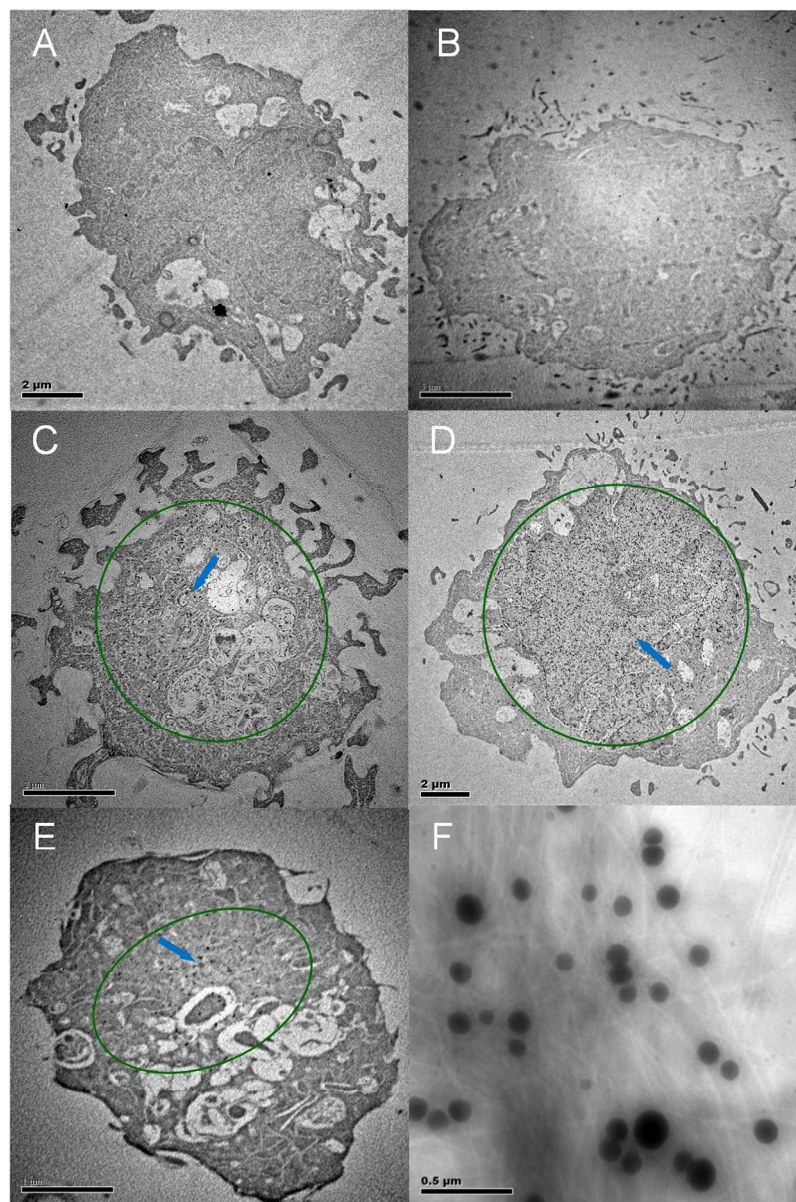


Figure 2. TEM photomicrographs of endogenous SeNPs formation in H157 cells (green cycle). (A) without selenite treatment; (B) 0 h selenite exposure; (C) 24 h selenite exposure; (D) 36 h selenite exposure; (E) 72 h selenite exposure. Blue arrows point to endogenous SeNPs on image. (F) TEM image of SeNPs isolated from H157 cells.

363x540mm (200 x 200 DPI)

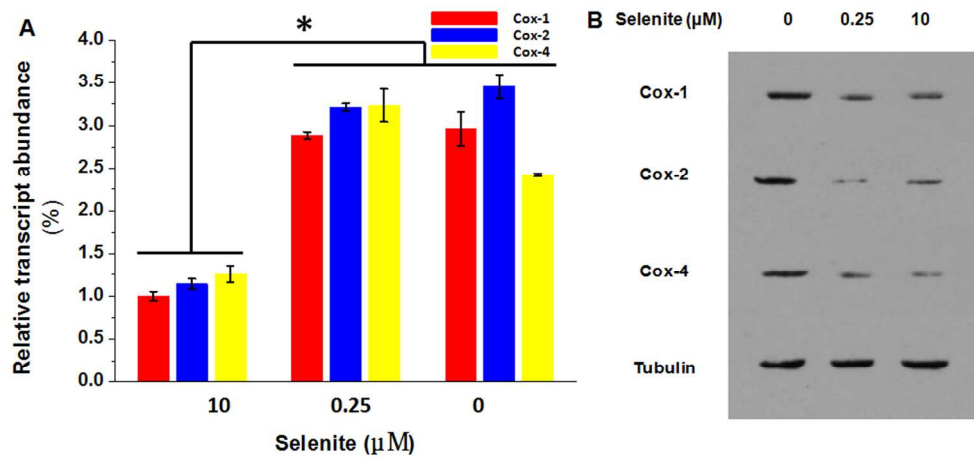


Figure 3. Relative transcript abundance of Cox-1, Cox-2 and Cox-4 in H157 cells (A). Western blotting images of Cox-1, Cox-2 and Cox-4 level in H157 cells (B).  
175x84mm (300 x 300 DPI)

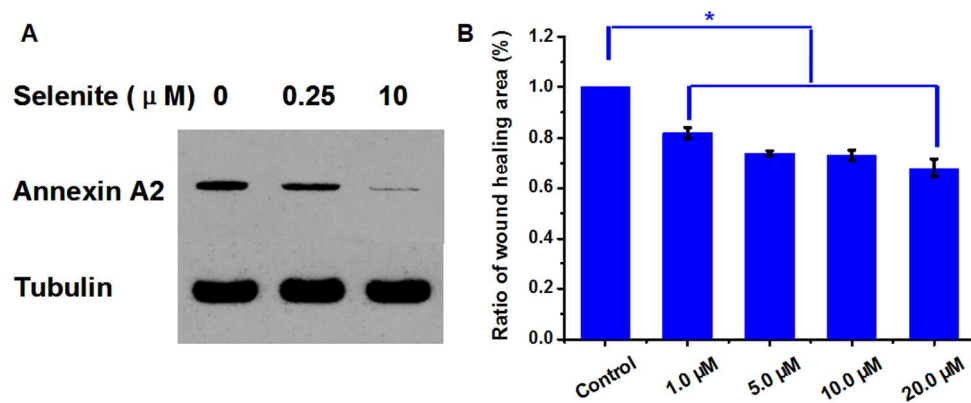
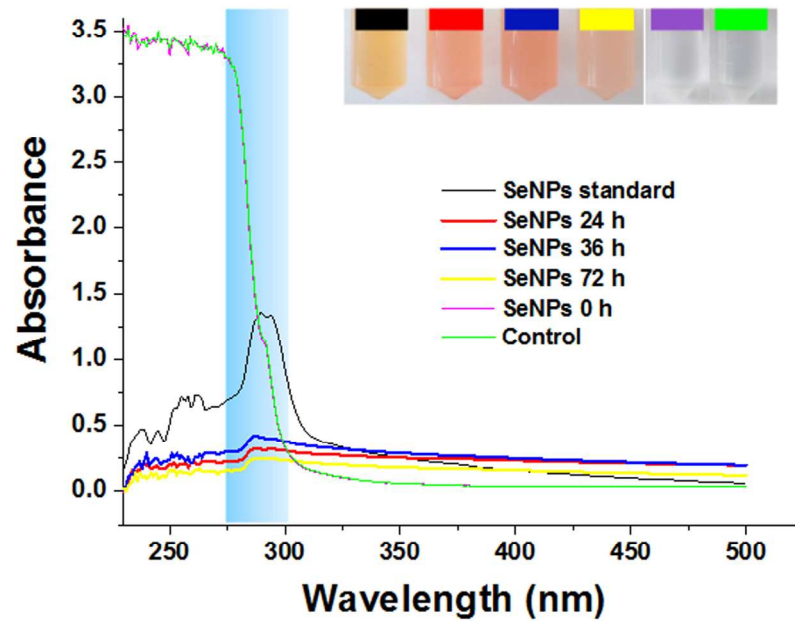


Figure 4. Suppressive effect of endogenous SeNPs mediated annexin A2 decreasing on the invasion and migration potential of H157 cells. A: Representative Western blotting images of annexin A2 level in H157 cells; B: Wound healing in DMEM cultures after 24h incubation with 0–20  $\mu\text{M}$  of selenite. 179x80mm (300 x 300 DPI)



Dynamics of SeNPs in cell line H157 at the time point of 0 h, 24 h, 36 h and 72 h (n=3). Treatment without selenite is shown as green line. The region of SeNPs absorption is indicated by blue column (around 275 nm).

247x176mm (300 x 300 DPI)

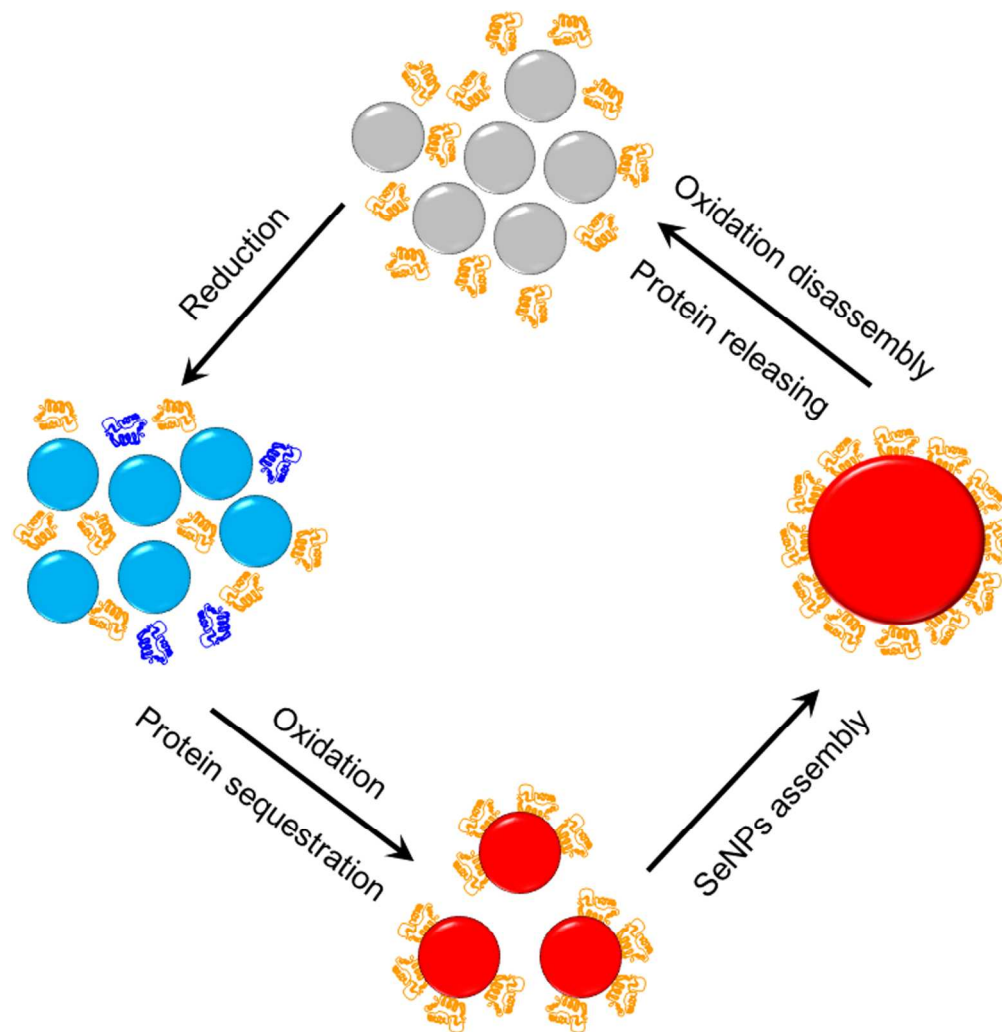


Figure 6. Putative pathway one: dynamic equilibrium of SeNPs metabolism in cancer cells. Selenide ions; Elemental selenium; Selenite; Proteins sequestered by SeNPs; Newly involved proteins.  
267x273mm (300 x 300 DPI)

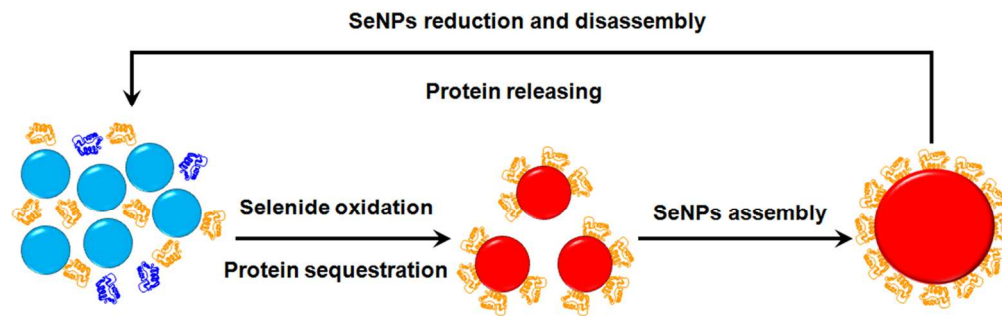


Figure 7. Putative pathway two: dynamic equilibrium of SeNPs metabolism in cancer cells. Selenide ions; Elemental selenium; Proteins sequestered by SeNPs; Newly involved proteins.  
122x38mm (300 x 300 DPI)